

Article

A Novel Flux Focusing Magnetically Geared Machine with Reduced Eddy Current Loss

Jin Liu ^{1,2}, Wenxiang Zhao ^{1,2,*}, Jinghua Ji ^{1,2}, Guohai Liu ^{1,2} and Tao Tao ^{1,2}

¹ School of Electrical and Information Engineering, Jiangsu University, Zhenjiang 212013, China; liujin23.8@qq.com (J.L.); jjh@ujs.edu.cn (J.J.); ghliu@ujs.edu.cn (G.L.); taotao198735@163.com (T.T.)

² Jiangsu Key Laboratory of Drive and Intelligent Control for Electric Vehicle, Zhenjiang 212013, China

* Correspondence: zwx@ujs.edu.cn; Tel.: +86-511-8879-1960

Academic Editor: K.T. Chau

Received: 18 July 2016; Accepted: 27 October 2016; Published: 2 November 2016

Abstract: This paper proposes a novel flux focusing magnetically geared (MG) machine for wind power generation, considering the permanent magnets (PMs) eddy current loss and the balance between the pull-out torque of MG machine and the back-electromotive force (EMF) of the PM brushless machine. The PM eddy current loss in the two rotors of the conventional surface-mounted MG machine is calculated and analyzed by using finite-element method. By adopting serial-spoke structure in the inner rotor, a novel rotor structure for a MG machine is proposed to reduce the PM eddy current loss. Moreover, in order to balance the pull-out torque and the back-EMF, several serial-spoke structures and the main design parameters are investigated. Then, a quantitative comparison between the proposed topology and the conventional surface-mounted MG machine is performed. The analysis results indicate that the PM eddy current loss of the proposed MG machine can be significantly reduced and its pull-out torque and back-EMF can be balanced well.

Keywords: finite-element method; eddy current loss; magnetic gear; serial-spoke structure; torque; back-electromotive force

1. Introduction

With the increase of energy problems and environmental pollution, wind power as an abundant, clear, renewable energy resource has gained more and more attention. Wind power generation can be classified as constant speed constant frequency and variable speed constant frequency. Several types of generators have been adopted or proposed in both systems, such as squirrel-cage induction generators [1], conventional synchronous generators [2], switched reluctance generators [3], and permanent magnet (PM) generators [4]. In fact, a mechanical gearbox and a medium or high speed machine is often engaged to match the low speed of wind turbine and relatively high rotor speed of generator. These geared wind turbine systems exhibit certain advantages such as high generator efficiency and light weight [5]. However, mechanical gears will increase the cost of manufacture and maintenance, reduce robustness. As an alternative, the direct-drive wind power PM generator has become more and more attractive due to its lower part count, simplicity and higher reliability prospects. Nevertheless, for large wind turbines with low-speed high-torque operation, the direct-drive wind power PM generator needs a bulky size with a very large pole number. Therefore, the economic incentive for a shift from geared systems to direct-drive systems seems insufficient.

In recent years, magnetically geared (MG) machines have attracted much attention [6–19]. MG machines incorporate a PM brushless machine and a magnetic gear into one volume. Compared with mechanical gears, MG machines can offer significant potential advantages, namely reduced acoustic noise, vibration, maintenance, improved reliability, inherent overload protection, and physical isolation between the input and output shafts. However, in order to obtain high torque density,

MG machines adopt a large number of rare-earth PMs, which lead to high PM eddy current loss. The losses may cause significant amount of heat generated in the PMs, resulting in partial irreversible demagnetization of the rare-earth PMs. Moreover, the eddy currents in the PMs may also affect the flux density distributions in the air-gap. Therefore, it is very necessary to reduce PM eddy current loss when designing a MG machine.

Recently, several papers have covered the topic of MG machine eddy current loss. Reference [20] proposed a convenient approach for calculation and analysis, while the magnetic flux barriers in the outer rotor are designed to reduce the eddy current loss based on the limitation of sub-harmonics in [21]. Nevertheless, these works devoted to reducing eddy current loss only consider the MG machine without integrated PM brushless machine. When a MG machine is integrated into a PM brushless machine, it is hard to balance the pull-out torque of MG machine and the back-EMF of the PM brushless machine due to the two air gaps of inner and middle. It has been known that the surface mounted-PM MG machines are immune to this problem, but the interior-PM MG machines suffer from this problem although their PM eddy current loss is much lower than the surface mounted machine. In fact, the interior PM structure can reduce PM eddy current loss, but the pull-out torque of the inner-rotor in [22] is reduced by 22% as compared with the surface-mounted MG machine having the same volume of rare-earth PMs.

The purpose of this paper is to propose a novel flux focusing structure MG machine considering the PM eddy current loss and the balance between the pull-out torque of MG machine and the back-EMF of the PM brushless machine. Section 2 will be devoted to describe the loss analysis, configurations of the existing and proposed topologies. Consequently, in Section 3, the parametric optimization analysis focusing on eddy current loss, torque, and back-EMF for the proposed topology will be presented. Then, by using finite-element method (FEM), the performances of the proposed and existing MG machines will be comparatively analyzed in Section 4. Finally, some conclusions will be drawn in Section 5.

2. Topology and Loss Analysis

As shown in Figure 1, a fault-tolerant magnetic-gear PM machine was proposed in [23]. It has two surface-mounted PM arrays on the inner rotor (high speed) and outer rotor (low speed). Also, the stator windings are integrated as a PM brushless machine with the inner rotor. Both the stationary ring pieces and the rotor cores are laminated with 0.35 mm silicon steel.

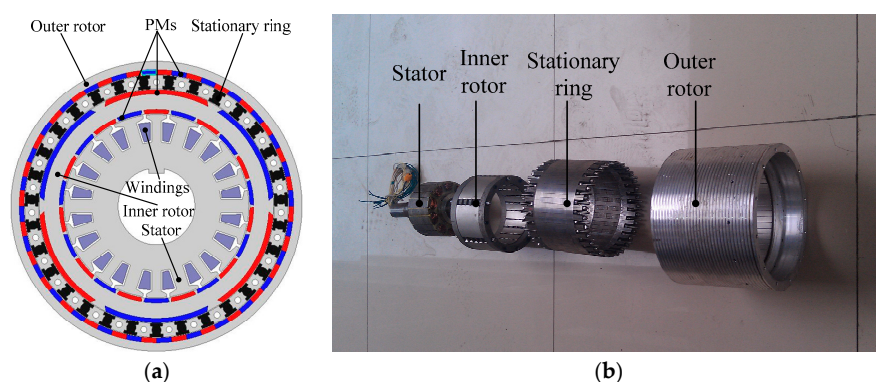


Figure 1. Existing machine: (a) cross section; and (b) prototype. PMs: permanent magnets.

The layout of the proposed machine is shown in Figure 2. The principle of the MG machine relies on the use of stationary ring pieces to modulate the magnetic fields generated by two sets of PMs. According to [9], the gearing ratio is given by:

$$G_r = (nP_h + kN_s)/nP_h, N_s = P_h + P_l, n = 1, 3, 5, \dots, k = 0, \pm 1, \pm 2, \pm 3, \dots, \pm \infty \quad (1)$$

where P_h is the PM pole-pairs of the inner rotor, P_l is the PM pole-pairs of the outer rotor, and N_s is the number of modulating segments. In order to transmit torque at different speeds, the PM pole-pairs of the outer rotor should be equal to the pole-pairs of the space harmonic. Since the combination of $n = 1$ and $k = -1$ will result in the highest asynchronous space harmonic, the gearing ratio can be obtained by $G_r = (N_s - P_h)/P_h$.

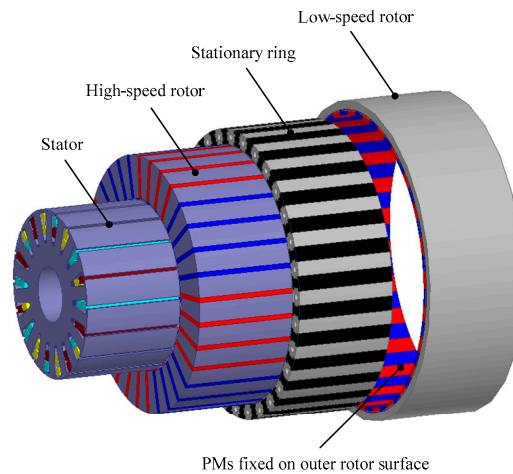


Figure 2. Proposed structure.

The FEM is used to predict PM eddy current loss of the surface-mounted MG machine. The eddy current loss of each part of the surface-mounted MG machine is shown in Figure 3. When the inner rotor rotates at the rated speed, it can be observed that the stationary ring loss is significantly higher than the PM eddy current loss. Moreover, the PM eddy current loss in the inner rotor is significantly higher than that in the outer rotor. It is known that the eddy current loss of the interior PM structure is lower than that of surface-mounted PM structure. Moreover, the eddy current losses in magnets can be reduced by segmentation of magnets [24]. Thus, it is possible to reduce the PM eddy current loss by changing the inner rotor to an interior PM structure with segmentation of the magnets.

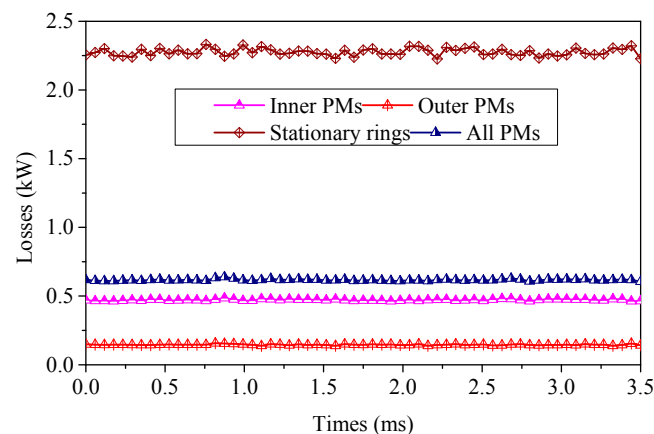


Figure 3. Losses of surface-mounted magnetically geared (MG) machine with inner rotor 5400 r/min.

3. Parameters Optimization

3.1. Optimization Goal

The purpose of this optimization is that the proposed MG machine can obtain higher torque and lower eddy current loss compared with the existing surface-mounted one.

The machine contains two torque components during its operation.

- The magnetic torque results from the magnetic gearing action of the high-speed rotor and the low-speed rotor, just like in magnetic gear.
- The electromagnetic torque is generated, primarily, as a consequence of interaction between the high-speed rotor and the field generated by the stator windings as in PM brushless machine.

In order to balance the maximum torque capability of the MG machine and the electrical machine components of a magnetic gear, the stator load factor γ_i is selected to ensure that PM brushless machine and magnetic gear components of the MG machine are well matched.

$$\gamma_i = -G_r T_i / T_m \quad (2)$$

where G_r is the gear ratio of the machine, T_i is the rated stator torque, and T_m is the stall torque of the low speed rotor. Considering the stability and the optimization, it can be known from (2) that the stator load factor should be above 0.8 and less than 1.0 [25].

3.2. Pole-Slot Selection

Similar to the conventional PM brushless machines, the MG machines can generate electromagnetic torque as a result of the interaction of the high speed rotor PM fundamental fields and stator windings. When the number of the out pole-pairs is constant, the different numbers of the inner rotor pole-pairs result in the different gear ratios. In a well-balanced design, the electromagnetic torque can be amplified by a factor of G_r to the magnetic torque on the low speed rotor, which significantly increases the machine torque density. From a different perspective, G_r determines how much electromagnetic torque is required in order to harness a given input low speed rotor torque, and G_r is a function of P_h and P_l . The pole selections of inner PMs determines the gear ratio G_r when the P_l is determined as 27. In order to obtain higher pull-out torque, when the gear ratio G_r , winding factor and the dimensional constraints in Table 1 are considered, 3 and 4 appear to be two possible pole combinations of the inner pole-pairs.

Moreover, the pole-slot selection of the inner brushless machine will have an effect on the wave distortion of the back-EMF and the torque ripple. Considering the winding factor and the dimensional constraints in Table 1, the 6/9 and 8/18 appear to be two possible pole-slot combinations.

Table 1. Fixed design parameters of the machine.

Parameters	Value	Units
Outer rotor outside radius r_{s_out}	94.7	mm
Stationary ring outside radius r_{s_in}	85.7	mm
Inner rotor outside radius r_{s_s}	76	mm
Stator radius yoke r_y	17	mm
Stator radius r_s	50.5	mm
Length of air gap t_{brg}	0.5	mm
PMs material	Nd-Fe-B	–
Magnet remanence	1.23	T
Grades of steel	0.35 mm silicon steel	–

In order to examine the relationship between the machine torque capabilities and G_r , also the relationship between the wave distortion of the back-EMF and pole-slot selection, the proposed MG machine is optimized to improve torque performance and reduce wave distortion of back-EMF. As shown in Figures 4 and 5, a few interesting conclusions can be drawn.

- For the same P_l number, the 8/18 combination invariably gives higher torque than the 6/9 combination due to the increased G_r .
- The MG machines with higher stator slots can be realized with a lower torque ripple.

- The higher stator slots can alleviate wave distortion and offer high peak values of the back-EMFs.

Therefore, the MG machines with 18 stator slots can improve wave distortion and offer a more nearly rectangular shape. Based on the above analysis, a final design with 8-poles ($P_h = 4$), 18-slots, and $P_l = 27$ is preferred.

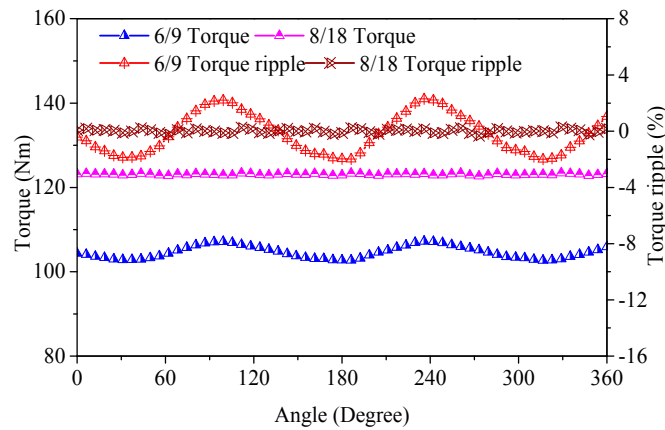


Figure 4. Torques and torque ripples with different pole-slot selection.

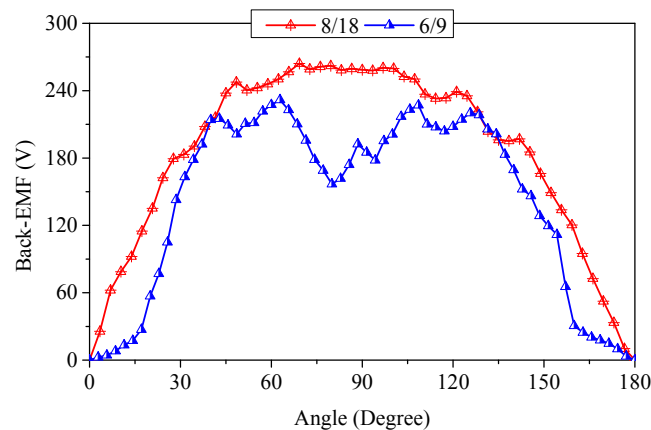


Figure 5. Back-electromotive forces (EMFs) with different pole-slot selection.

3.3. Spoke Serial Number Selection

The maximum stall torque of the single spoke-type MG machine in [22] is 27 Nm, while that of the surface-mounted one is 32 Nm, which is 18.5% higher than that of the single spoke-type MG machine. Moreover, the single spoke-type MG machine is not suitable to be integrated into a PM machine because it is hard to balance the pull-out torque of MG machine and the back-EMF of the PM brushless machine. However, the newly proposed series spoke-type structure can solve this problem, also reducing the PM eddy current loss.

Figure 6 shows the four spoke PM structures. The eddy current loss can be reduced by segmenting PMs although the same amount of PMs and the same radial thickness are retained. It can be seen from Figure 7 that the magnetic path direction is constant even though the PMs are divided into segmentations and evenly distributed on the inner rotor. However, as the segment of the series spoke structures increases, the flux density near the stator winding will increase, as shown in Figure 8. Furthermore, the increased flux density results in higher back-EMF. Figures 9 and 10 show the changes about the back-EMF, stator load factor γ_i , torque, and eddy current loss with the increase of the serial number. It can be seen from Figure 9 that the back-EMF increases with the increase of the serial number,

but the coefficient γ_i does not increase due to the lower torque of the single serial spoke. It can also be known that as the segment number increases, the decrease of eddy current loss and the increase of torque proceed more slowly. However, the structures with more segment numbers have significantly improved performance compared with the single serial spoke structure. It can be concluded that the four segment series structure is very effective to balance pull-out torque and back-EMF.

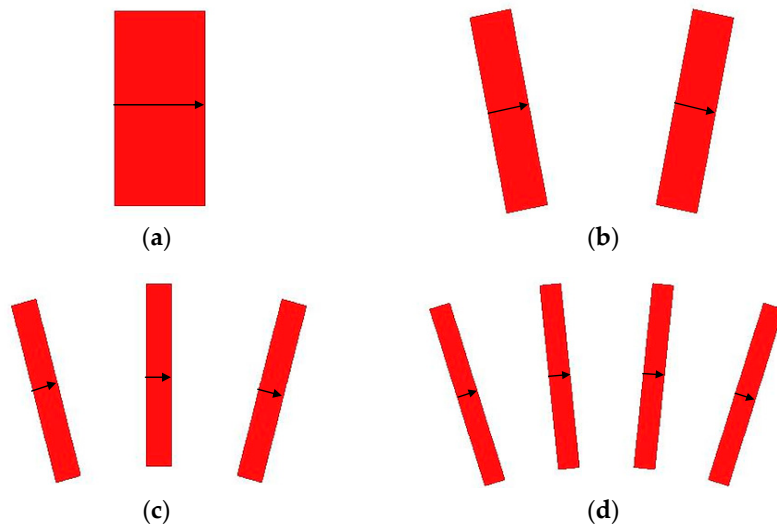


Figure 6. Four inner rotor spoke-type structures: (a) one segment; (b) two segments; (c) three segments; and (d) four segments.

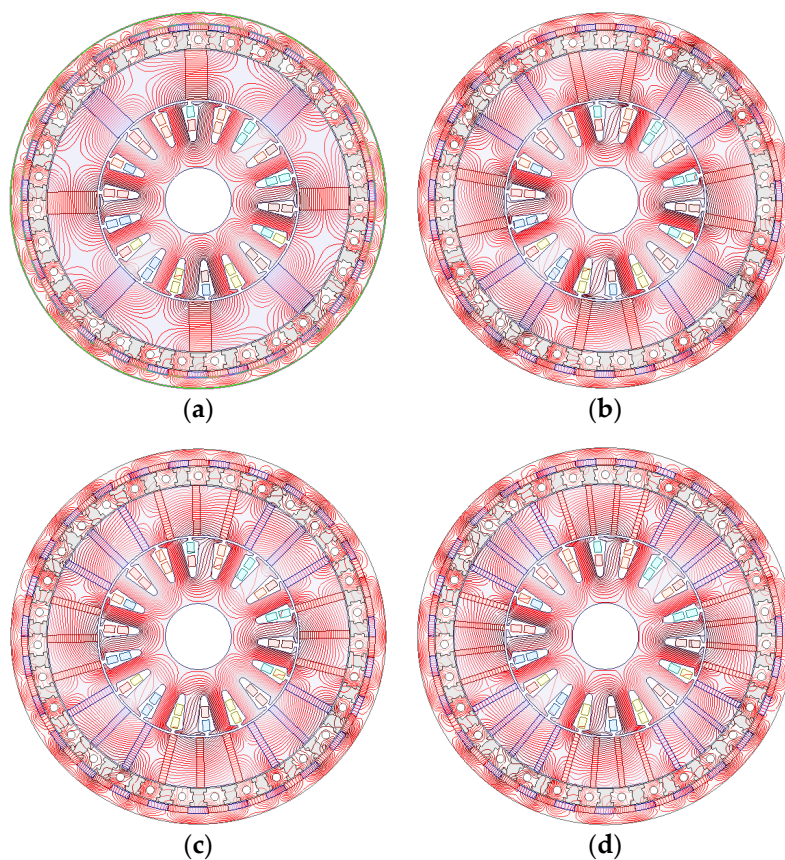


Figure 7. Flux lines of four spoke-type structures with no load: (a) one segment; (b) two segments; (c) three segments; and (d) four segments.

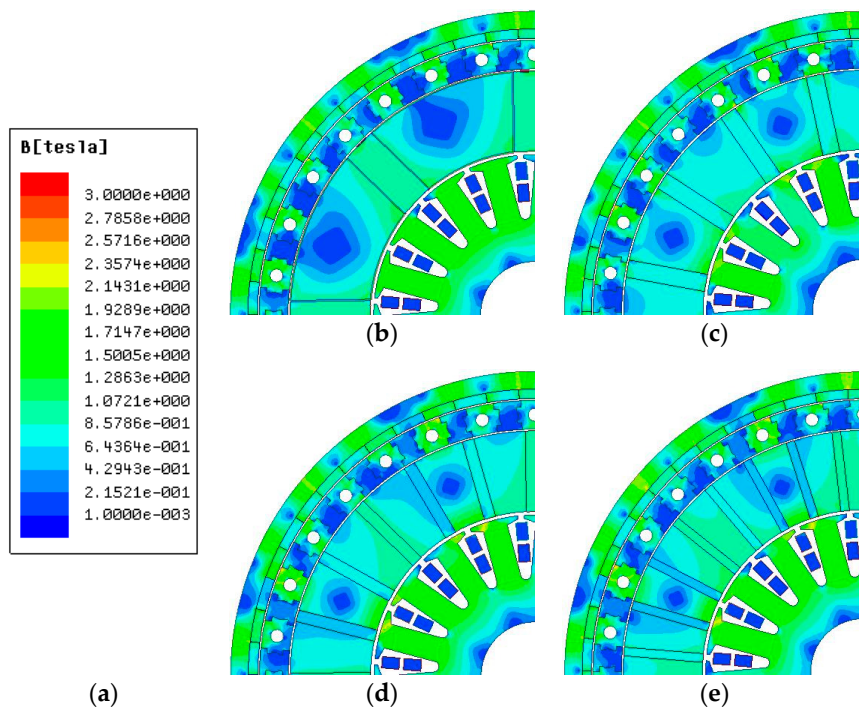


Figure 8. Flux density of four spoke-type structures with no load: (a) scale (b) one segment; (c) two segments; (d) three segments; and (e) four segments.

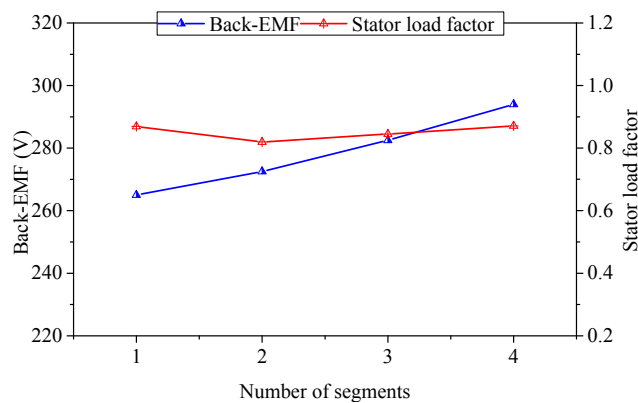


Figure 9. Back-EMF and stator load factor with different spoke-type structures.

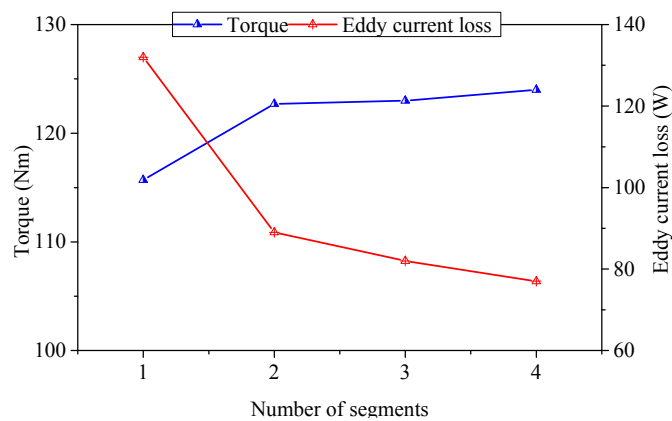


Figure 10. Torque and eddy current loss with different spoke-type structures.

It is known that the method of splitting PMs into sections appears beneficial only when the PM is a relatively small percentage of the steel and the pole number is low. The four inner structures have the same PM amount, so the PM is a relatively small percentage of the steel after splitting the PM into sections. Actually, splitting segments does not increase the pole number of the inner rotor as shown in Figure 6, just changing the magnetic flux density distribution of inner rotor. The changed magnetic flux density distribution improves the back-EMF, then improving the electromagnetic torque. Also, the pull-out torque increases after modulation. It should be noted that the diameter is the design limitations in the design process. For the motor with a small diameter, splitting the PM into sections will improve the torque. In order to compare with the existing motor, the proposed structure has the larger diameter. Hence, the effect of the proposed structure is not particularly obvious, but the proposed structure has greater advantages as compared with the existing surface-mounted machine.

3.4. Final Design

Table 2 summarizes the final design for the proposed four segments series structure, which are defined in Figure 11. Based on the FEM, the magnetic field and flux density distributions of the optimized machine under full-load condition are predicted as shown in Figure 12. The flux lines of the inner rotor connected the stator windings and the outer rotor crossed the modulator, which is beneficial for torque production of the inner rotor and back-EMF.

Table 2. Optimized variables.

Parameters	Value	Units
Number of stator slots	18	–
Number of pole-pairs on inner rotor	4	–
Number of segments	4	–
Number of pole-pairs on outer rotor	27	–
Number of stationary rings	31	–
Stator tooth thickness t_{stt}	18.4	mm
Slot tip r_{stp} (fraction of tooth thickness)	0.86	–
Slot opening θ_{sto} (fraction of slot pitch)	0.12	–
Stator yoke thickness t_{sty}	13.3	mm
Stator parameter r_{st}	1.66	mm
Length of inner rotor PMs t_{mh}	25	mm
Thickness of inner rotor PMs h_m	2.75	mm
Rotor magnet span to pole embrace θ_{s2}/θ_{s1}	0.89	–
Stationary ring parameter θ_{m1}	1.1	°
Stationary ring span to pole embrace θ_{m2}/θ_{m3}	1	–
Stationary ring parameter d_{m1}	4	mm
Stationary ring parameter d_{m2}	6	mm
Stationary ring parameter h_s	2	mm
Thickness of outer rotor PMs t_{rm}	3	mm
Thickness of outer rotor yoke t_{ry}	5.5	mm
Stack length	60	mm

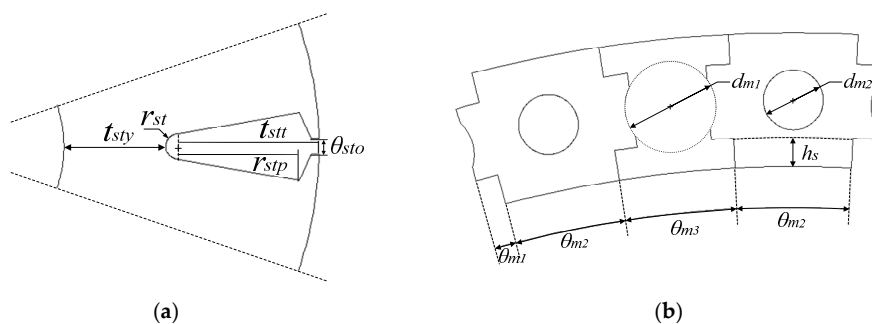


Figure 11. Cont.

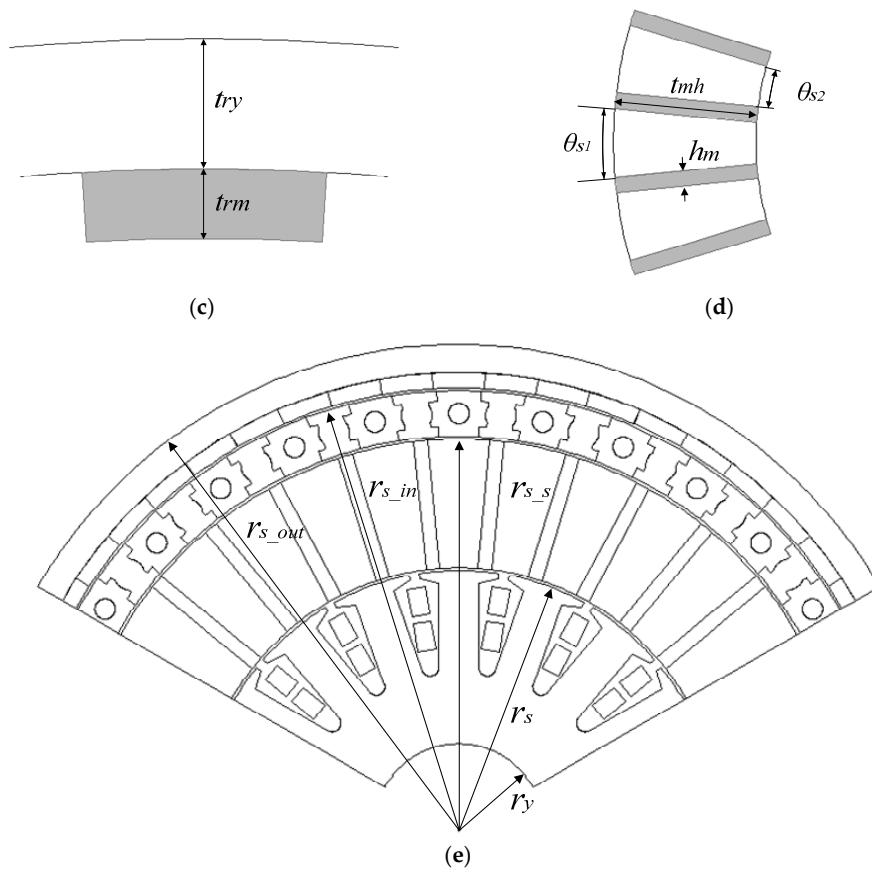


Figure 11. Geometric variables input to finite-element method: (a) stator; (b) stationary ring; (c) outer rotor; (d) inner rotor; and (e) radius of parameters.

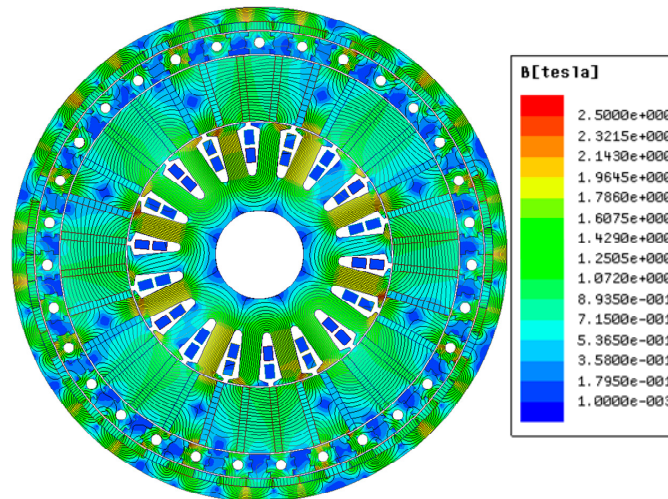


Figure 12. Flux density and field lines under full load with rated stator current.

Figure 13 shows the air-gap flux density and its harmonic spectrum in the outer air-gap due to the inner rotor PMs only. It can be found that the highest asynchronous harmonic component is the 27 pole-pairs one. Comparatively, Figure 14 shows the air-gap flux density and its harmonic spectrum in the middle air-gap due to the outer rotor PMs only. It can be seen that the highest asynchronous harmonic component is the four pole-pairs one. Therefore, it can be concluded that the most significant

space harmonic is successfully modulated by modulating segments from four pole-pairs in the air-gap adjacent to the inner rotor to 27 pole-pairs in the air-gap adjacent to the outer rotor. The analysis results of the harmonic spectrum proves the feasibility of the proposed MG machine in theory.

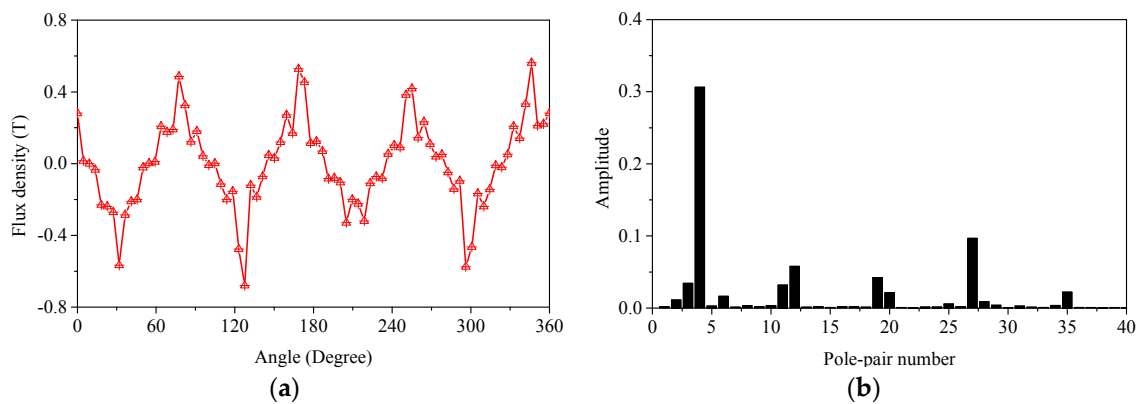


Figure 13. Airgap flux density in the outer airgap due to the inner rotor PMs: (a) flux density; and (b) harmonic spectrum.

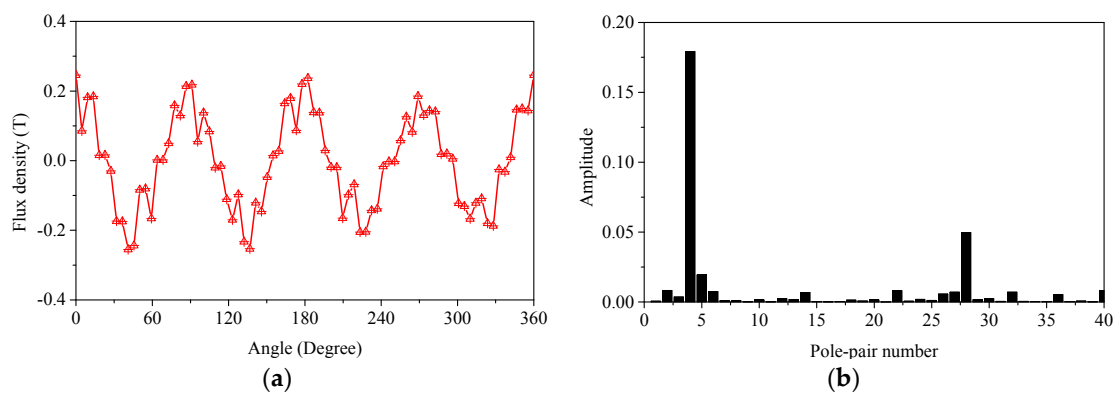


Figure 14. Airgap flux density in the inner airgap due to the outer rotor PMs: (a) flux density; and (b) harmonic spectrum.

4. Performance Evaluation

4.1. Back-EMF

The proposed inner structure can connect the magnetic circuit of the outer PMs pasted the modulation ring and the stator windings. Thus, the proposed machine integrated PM brushless machine can reduce magnetic flux leakage effectively. The simulated back-EMFs of the existing and proposed MG machines at the speed of 520 r/min (inner rotor) are shown in Figure 15, respectively. It can be seen that the total harmonic distortion (THD) of the proposed one is higher than that of the existing one. Since the existing machine is a five-phase machine and the proposed machine is a three-phase one, the comparison of the magnitude of the back-EMFs is unfair. Thus, the stator load factor γ_i is adopted for a fair comparison when the two machines have the same power. As listed in Table 3, the proposed machine has the lower stator load factor γ_i than the existing one. The measured back-EMFs of the existing machine at the speed of 520 r/min (inner rotor) are shown in Figure 16, which agrees with the simulated one.

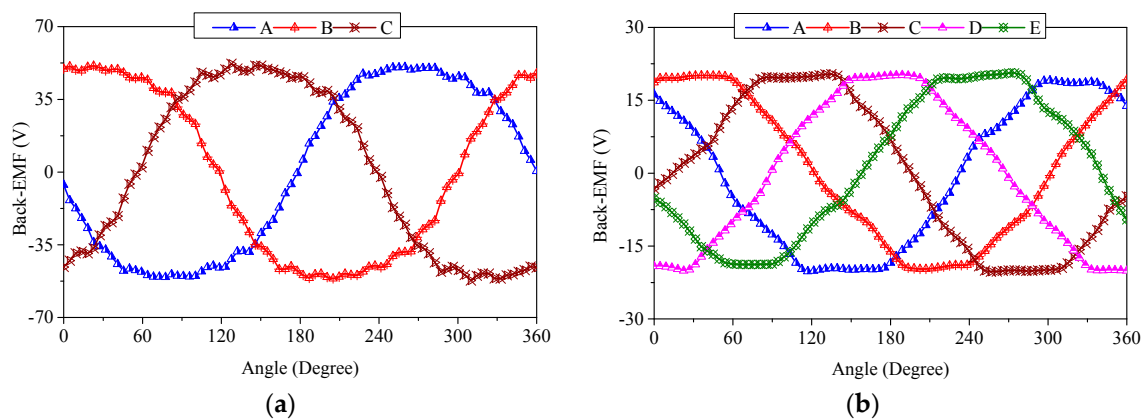


Figure 15. Back-EMF waveforms: (a) proposed and (b) existing.

Table 3. Performance comparison of two machines.

Descriptions	Existing	Proposed
Torque (Nm)	123.7	122.3
Volume (L)	1.64	1.64
Torque density (kNm/m ³)	76	75.1
Eddy current loss (W)	57	37
Core loss (W)	100	13
Stator load factor	0.91	0.85
Efficiency (%)	90	94
Power factor	0.93	0.93
Operating speed (r/min)	1200	1200

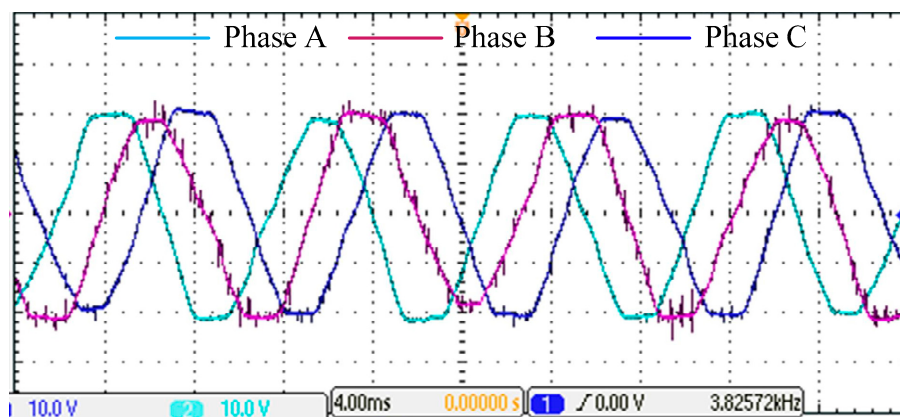


Figure 16. Measured back-EMF waveforms (4 ms/div, 10 V/div): the green line marks phase A, the red line marks phase B and the blue line marks phase C.

4.2. Torque

In order to improve torque performance, the torque–angle relationship is considered, as shown in Figure 17. It can be known that the maximum torques of the outer rotor and the inner rotor are 122.3 Nm and 17.9 Nm, respectively. Their ratio is 6.83, which has a good agreement with the gearing ratio of 6.75. According to the machine dimensions listed in Table 1, the torque density of 75.1 kNm/m³ can be calculated.

The cogging torque of the inner rotor is shown in Figure 18. It can be seen that the cogging torque is relatively high, which results in high torque ripple of the inner rotor as shown in Figure 19. It has been known that the cogging torque ripple of the MG machine is approximately related to the inverse of the smallest common multiple (N) of the number of the inner rotor poles ($2 \cdot P_{ri}$) and the number of

modulating segments (N_s). Hence, $N = 248$ is adopted in this work. Although this theoretical design is obtained, the cogging torque is still relatively high, which is caused by the higher segments of inner PMs.

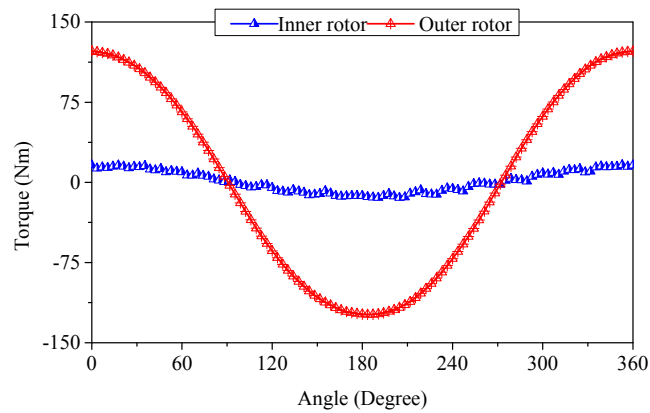


Figure 17. Torque–angle relationship.

The full load torque of the proposed machine with the rated current of 10 A is shown in Figure 19. It can be seen that the inner torque ripple is high due to the significant cogging torque. However, the average torque on the inner rotor is almost zero in spite of the high cogging torque, and the outer torque ripple is very small. It can be concluded that the proposed machine can operate at a steady speed.

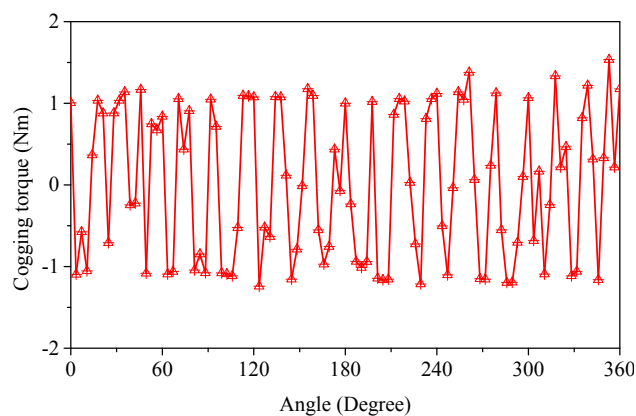


Figure 18. Cogging torque.

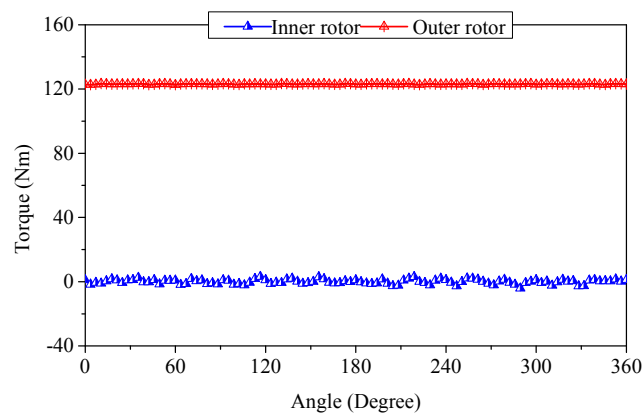


Figure 19. Full load torques.

4.3. Loss And Efficiency

When considering the eddy current loss and neglecting the stationary ring loss, the efficiency of the proposed machine can be approximated as:

$$\eta = P_{out}/(P_{out} + P_{core} + P_c + P_{ec}) \times 100\% \quad (3)$$

where P_{out} is out power, P_{core} is core loss, P_c is copper loss, and P_{ec} is eddy current loss. When the proposed machine is supplied with rated current of 10 A and the rated speed 1200 r/min of inner rotor, the eddy current loss and core loss are shown in Figure 20. The eddy current loss and core loss are about 13 W and 37 W, respectively. It can be concluded that the loss is mainly induced in the stator and two rotors. The efficiency of the proposed machine is 94%.

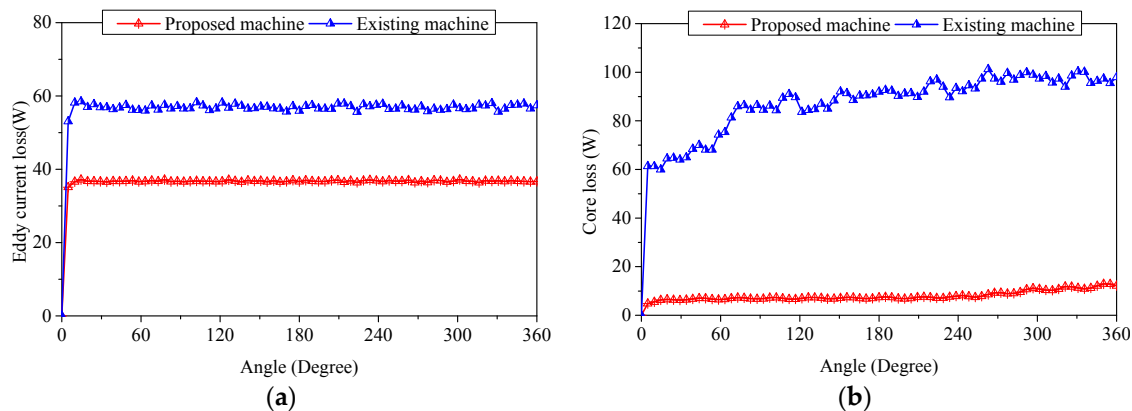


Figure 20. Losses at the full operation: (a) eddy current loss; and (b) core loss.

4.4. Comparison

In order to further evaluate the proposed machine, it is quantitatively compared with the existing one. For a fair comparison, both machines adopt the same outer radius and the same slot-fill factor. As listed in Table 3, it can be seen that the proposed machine has slightly lower torque density, but has much lower loss than the existing one. Moreover, the stator load factor of the proposed machine is less, but its value is over 0.8.

5. Conclusions

This paper has proposed and designed a novel flux focusing structure MG machine in order to minimize the eddy current loss and balance between the pull-out torque and back-EMF. The configuration and parameters optimization of the proposed MG machine have been discussed. By adopting interior PM structure, segmentation of PMs, the eddy current loss has been reduced effectively and the problem between the pull-out torque and back-EMF can be very effectively balanced. Then, by using the 2D-FEM, the quantitative analysis of the proposed topology has verified that the proposed MG machine can balance pull-out torque and back-EMF well. The comparison between the proposed topology and the surface-mounted MG machine reveals that the proposed MG machine can offer 35% lower PM eddy current loss and 87% lower core loss.

Acknowledgments: This work was supported by the National Natural Science Foundation of China (Projects 51477068 and 51422702), by the Qing Lan Project of Jiangsu Province, and by the Priority Academic Program Development of Jiangsu Higher Education Institutions.

Author Contributions: This paper is a result of the full collaboration of all the authors. Jin Liu, Wenxiang Zhao, and Jinghua Ji have contributed developing ideas and analytical model. Guohai Liu and Tao Tao were responsible for the guidance and a number of key suggestions.

Conflicts of Interest: The authors declare no conflict of interest.

References

1. Duong, M.; Grimaccia, F.; Leva, S.; Mussetta, M.; Le, K. Improving transient stability in a grid-connected squirrel-cage induction generator wind turbine system using a fuzzy logic controller. *Energies* **2015**, *8*, 6328–6349. [[CrossRef](#)]
2. Wang, D.; Liu, C.; Li, G. An optimal integrated control scheme for permanent magnet synchronous generator-based wind turbines under asymmetrical grid fault conditions. *Energies* **2016**, *9*, 307. [[CrossRef](#)]
3. Shin, H.; Park, K.; Lee, K. A non-unity torque sharing function for torque ripple minimization of switched reluctance generators in wind power systems. *Energies* **2015**, *8*, 11685–11701. [[CrossRef](#)]
4. Beik, O.; Schofield, N. An offshore wind generation scheme with a high-voltage hybrid generator, HVDC interconnections, and transmission. *IEEE Trans. Power Deliv.* **2016**, *31*, 867–877. [[CrossRef](#)]
5. Wang, R.J.; Brönn, L.; Gerber, S.; Tlali, P.M. Design and evaluation of a disc-type magnetically geared PM wind generator. In Proceedings of the 2013 4th International Conference on Power Engineering, Energy and Electrical Drives (POWERENG), Istanbul, Turkey, 13–17 May 2013; pp. 1259–1264.
6. Chau, K.T.; Zhang, D.; Jiang, J.Z. Design of a magnetic-geared outer-rotor permanent-magnet brushless motor for electric vehicles. *IEEE Trans. Magn.* **2007**, *43*, 2504–2506. [[CrossRef](#)]
7. Rashidi, H.; Pishdad, D. Integrated multispeed magnetic gears: A novel approach to design of magnetic transmission systems. *IEEE Trans. Magn.* **2014**, *51*, 1–8. [[CrossRef](#)]
8. Zhao, W.; Liu, J.; Ji, J.; Liu, G.; Ling, Z. Comparison of coaxial magnetic gears with and without magnetic conducting ring. *IEEE Trans. Appl. Supercond.* **2016**, *26*, 1–5. [[CrossRef](#)]
9. Atallah, K.; Howe, D. A novel high-performance magnetic gear. *IEEE Trans. Magn.* **2001**, *37*, 2844–2846. [[CrossRef](#)]
10. Liu, C.; Chau, K.T. Electromagnetic design of a new electrically controlled magnetic variable-speed gearing machine. *Energies* **2014**, *7*, 1539–1554. [[CrossRef](#)]
11. Shin, H.M.; Chang, J.H. Analytical magnetic field calculation of coaxial magnetic gear with flux concentrating rotor. *IEEE Trans. Magn.* **2016**, *52*, 1–4. [[CrossRef](#)]
12. Zhang, X.; Liu, X.; Wang, C.; Chen, Z. Analysis and design optimization of a coaxial surface-mounted permanent-magnet magnetic gear. *Energies* **2014**, *7*, 8535–8553. [[CrossRef](#)]
13. Ho, S.L.; Wang, Q.; Niu, S.; Fu, W.N. A novel magnetic-geared tubular linear machine with halbach permanent-magnet arrays for tidal energy conversion. *IEEE Trans. Magn.* **2015**, *51*, 1–4.
14. Chen, Y.; Fu, W. A novel hybrid-flux magnetic gear and its performance analysis using the 3-D finite element method. *Energies* **2015**, *8*, 3313–3327. [[CrossRef](#)]
15. Chen, M.; Chau, K.T.; Li, W.; Liu, C.; Qiu, C. Design and analysis of a new magnetic gear with multiple gear ratios. *IEEE Trans. Appl. Supercond.* **2014**, *24*. [[CrossRef](#)]
16. Feng, N.; Yu, H.; Hu, M.; Liu, C.; Huang, L.; Shi, Z. A study on a linear magnetic-geared interior permanent magnet generator for direct-drive wave energy conversion. *Energies* **2016**, *9*, 487. [[CrossRef](#)]
17. Peng, S.; Fu, W.N.; Ho, S.L. A novel high torque-density triple-permanent-magnet-excited magnetic gear. *IEEE Trans. Magn.* **2014**, *50*, 1–4. [[CrossRef](#)]
18. Jing, L.; Liu, L.; Xiong, M.; Feng, D. Parameters analysis and optimization design for a concentric magnetic gear based on sinusoidal magnetizations. *IEEE Trans. Appl. Supercond.* **2014**, *24*, 1–5. [[CrossRef](#)]
19. Wang, L.; Shen, J.; Luk, P.C.K.; Fei, W.; Wang, C.; Hao, H. Development of a magnetic-geared permanent-magnet brushless motor. *IEEE Trans. Magn.* **2009**, *45*, 4578–4581. [[CrossRef](#)]
20. Zhang, Y.Q.; Lu, K.Y.; Ye, Y.Y. Permanent magnet eddy current loss analysis of a novel motor integrated permanent magnet gear. *IEEE Trans. Magn.* **2012**, *48*, 3005–3008. [[CrossRef](#)]
21. Tian, Y.; Liu, G.H.; Zhao, W.X.; Ji, J.H. Design and analysis of coaxial magnetic gear considering rotor losses. In Proceedings of the 2015 IEEE Magnetics Conference (INTERMAG), Beijing, China, 11–15 May 2015; pp. 1–4.
22. Rasmussen, P.O.; Andersen, T.O.; Joergensen, F.T.; Nielsen, O. Development of a high-performance magnetic gear. *IEEE Trans. Ind. Appl.* **2005**, *41*, 764–770. [[CrossRef](#)]
23. Liu, G.; Jiang, Y.; Ji, J.; Chen, Q.; Yang, J. Design and analysis of a new fault-tolerant magnetic-geared permanent-magnet motor. *IEEE Trans. Appl. Supercond.* **2014**, *24*. [[CrossRef](#)]

24. Huang, W.Y.; Bettayeb, A.; Kaczmarek, R.; Vannier, J.C. Optimization of magnet segmentation for reduction of eddy-current losses in permanent magnet synchronous machine. *IEEE Trans Energy Convers.* **2010**, *25*, 381–387. [[CrossRef](#)]
25. Gerber, S.; Wang, R.J. Design and evaluation of a magnetically geared pm machine. *IEEE Trans. Magn.* **2015**, *51*, 1–10. [[CrossRef](#)]



© 2016 by the authors; licensee MDPI, Basel, Switzerland. This article is an open access article distributed under the terms and conditions of the Creative Commons Attribution (CC-BY) license (<http://creativecommons.org/licenses/by/4.0/>).